# Removal of atmospheric features in near infrared spectra by means of principal component analysis and target transformation for the study of hydrated minerals on Mars

Geminale A.[1], Grassi D.[1], Altieri F.[1], Serventi, G.[2], Carli C.[1], Carrozzo F.G.[1], Sgavetti M.[2], Orosei R.[3], D'Aversa E.[1], Bellucci G.[1], Frigeri A.[1]

[1] IAPS Istituto di Astrofisica e Planetologia Spaziali, INAF Istituto Nazionale di AstroFisica, Via del Fosso del Cavaliere, 100-00133 Rome, Italy
[2] Department of Physics and Earth Sciences "Macedonio Melloni", University of Parma, Italy
[3] Istituto di Radioastronomia, Istituto Nazionale di Astrofisica, Via Piero Gobetti, 101, I-40129, Bologna, Italy

## Abstract

The aim of this work is to extract the surface contribution in the Martian visible/near-infrared spectra removing the atmospheric components by means of Principal Component Analysis (PCA) and target transformation (TT). The developed technique is suitable for separating spectral components in a data set large enough to enable an effective usage of statistical methods, in support to the more common approaches to remove the gaseous component. In this context, a key role is played by the estimation, from the spectral population, of the covariance matrix that describes the statistical correlation of the signal among different points in the spectrum. As a general rule, the covariance matrix becomes more and more meaningful increasing the size of initial population, justifying therefore the importance of sizable datasets. Data collected by imaging spectrometers, such as the OMEGA (Observatoire pour la Minéralogie, l'Eau, les Glaces et l'Activité) instrument on board the ESA mission Mars Express (MEx), are particularly suitable for this purpose since it includes in the same session of observation a large number of spectra with different content of aerosols, gases and mineralogy. The methodology presented in this work has been first validated using a simulated dataset of spectra to evaluate its accuracy. Then, it has been applied to the analysis of OMEGA sessions over Nili Fossae and Mawrth Vallis regions, which have been already widely studied because of the presence of hydrated minerals. These minerals are key components of the surface to investigate the presence of liquid water flowing on the Martian surface in the Noachian period. Moreover, since a correction for the atmospheric aerosols (dust) component is

also applied to these observations, the present work is able to completely remove the atmospheric contribution from the analysed spectra. Once the surface reflectance, free from atmospheric contributions, has been obtained, the Modified Gaussian Model (MGM) has been applied to spectra showing the hydrated phase. Silicates and iron-bearing hydrated minerals have been identified by means of the electronic transitions of $Fe^{2+}$ between 0.8-1.2 µm, while at longer wavelengths the hydrated mineralogy is identified by overtones of the OH group. Surface reflectance spectra, as derived through the method discussed in this paper, clearly show a lower level of the atmospheric residuals in the 1.9 hydration band, thus resulting in a better match with the MGM deconvolution parameters found for the laboratory spectra of Martian hydrated mineral analogues and allowing a deeper investigation of this spectral range.

*Keywords*: Mars, atmosphere, surface reflectance, OMEGA, mineralogy

## 1. Introduction

The main purpose of this work is to apply the PCA and the target transformation (TT) method to data acquired by imaging spectrometers on board space missions orbiting Mars, in order to remove the atmospheric contribution. This will allow for the isolation of the surface spectra in order to investigate hydrated mineral features. Imaging spectrometers measure a signal in the near-infrared spectral range that contains information about the atmosphere as well as about the surface. The measured spectra result in a combination of these different spectral contributions and a methodology is necessary to separate the atmospheric component from the surface reflectance. The high resolution spectral data provided between 0.4 and 2.5 µm by both the OMEGA (Observatoire pour la Minéralogie, l'Eau, les Glaces et l'Activité) and CRISM (Compact Reconnaissance Imaging Spectrometer for Mars) imaging spectrometers, on board the ESA/Mars Express and the NASA/MRO respectively, allow for the identification and mapping of different minerals (e.g., Bibring et al., 2004; Murchie et al., 2007a). However, while the electronic absorption features diagnostic of transitional elements bearing minerals (e.g., ferro-magnesian silicates) occur at wavelengths not affected by Mars atmospheric composition, the vibrational overtone absorptions bands due to water, $OH^-$, and $(CO_3)^{2-}$ in minerals overlap the absorption of water and $CO_2$ in the atmosphere. Therefore, an accurate removal of the atmospheric components (aerosols and gaseous species) is necessary to extract the actual surface contribution in the spectra. The standard processing approach to remove the atmospheric contribution is to divide the spectra by a scaled atmospheric spectrum measured across Olympus Mons (Langevin et al., 2005; McGuire et al.

2009). Then, the residual errors are suppressed by ratioing the target spectrum by a low spectral contrast reference spectrum of the same observational session (or cube), apparently without any relevant features and characterized by a smoother continuum (e.g., Bibring et al., 2005). Bakker et al. (2014) introduced a new method to obtain the surface reflectance deriving atmospheric transmission models (ATM) from the OMEGA image itself. This method has the advantage to take into account the seasonal and diurnal variability of the atmospheric gases ($CO_2$ and $H_2O$), but no attempt was made to correct for aerosols effects.

Bandfield et al. (2000) and D'Amore et al. (2013) have already applied the multivariate analyses techniques to the Thermal Emission Spectrometer (TES) on board the NASA Mars Global Surveyor satellite and to the Planetary Fourier Spectrometer (PFS) instrument on board the ESA Mars Express (MEx) spacecraft, respectively. The authors were able to properly recover the atmospheric contribution (dust and water ice clouds) to the observed radiation in the thermal/far-infrared spectral range. Glotch and Bandfield (2006) found the surface spectral components and atmospheric spectral shapes at Meridiani Planum applying the PCA and TT to the Miniature Thermal Emission Spectrometer (Mini-TES). Glotch and Rogers (2013) used factor analysis and TT to search for carbonate decompositions products on the surface of Mars. Smith at al. (2000) successfully separated the contribution of atmospheric and surface components in TES data assuming that each spectrum is a linear combination of its components. Thomas and Bandfield (2013) used the TT on CRISM data to confirm the presence of Mg-rich carbonates near Nili Fossae region on Mars, while Thomas et al. (2014) used the TT to identify diagnostic serpentine spectral features in the CRISM near-infrared data on the same Martian region. Klassen (2009) found a set of spectral end-members applying the PCA and TT to near infrared cube images of Mars acquired by the NASA Infrared Telescope Facility. In our work, we apply the same technique, hereafter called Surface Atmosphere Separation (SAS) method, to the OMEGA data in the near-infrared spectral range. In particular, we focused on surface reflectance spectra that show the hydrated absorption bands, which occur in the spectral range between 1.8 and 2.2 μm that is strongly influenced by the atmospheric absorption of $H_2O$ and $CO_2$.

Section 2 gives a short description of the OMEGA instrument and the set of data used in the present work. Section 3.1 summarizes the theoretical background of the PCA and target transformation approach, while the application of the method to a test case is shown in Section 3.2. Section 4 is devoted to the analysis of two OMEGA orbits passing through Nili Fossae (Section 4.2) and Mawrth Vallis (Section 4.3), where different mineral assemblages and the presence of phyllosilicates where already recognized (e.g., Poulet et al., 2005; Mustard, et al., 2007; Mangold et

al., 2007; Ehlmann et al., 2008; Poulet et al., 2008; Bishop et al., 2008; Noe Dobrea, et al., 2010). The presence of these minerals on the Noachian crust of Mars implies likely the presence of liquid water during the first billion year (e.g., Loizeau et al., 2007) and strong climate changes between the present time and the epoch in which phyllosilicates formed. The application of the multivariate analyses techniques to OMEGA spectra in order to remove the gaseous atmospheric components is completed by the removal of atmospheric dust component as described in Section 4.4. The spectral surface component classification and deconvolution are addressed in Section 5, where it is shown that the SAS method permits an improvement in the identification of the mineralogical phases by means of MGM, in particular for the investigation of hydrated mineralogy. Finally, the discussion and conclusions are in Section 6 and 7, respectively.

## 2. Instrument and dataset

In each resolved pixel (1.2x1.2 mrad instantaneous field of view, IFOV) OMEGA acquires a spectrum in 352 contiguous spectral elements (spectels) from 0.35 to 5.1 μm, with a spectral sampling ranging from 7 nm (in the visible and near infrared (VNIR) channel, between 0.38 and 1.05 μm) to 14 nm (short wavelength range, SWIR-C, between 0.93 and 2.73 μm) and 20 nm (SWIR-L, which covers the interval 2.55–5.1 μm). The signal-to-noise ratio (SNR) is > 100 over the whole spectral range (Bibring et al., 2004) for observations obtained in nadir mode and considering low solar zenith angles. The data products are organized in three-dimensional arrays (or cubes), with one spectral and two spatial dimensions (x, y, λ). Due to the MEx spacecraft elliptic orbit, the scan widths in each orbit are changed (16, 32, 64, 128 pixels) accordingly to the variation of the observing distance, e.g., 16 pixels are used for the low-elevation (<350 km, orbit peri-center) and consequently for high-resolution (300 m/pixels) observations, whereas the 128 pixels mode is adopted for elevations above 1500 km to provide wide images with spatial sampling greater than 2 km/pixel. Data and calibration software are publicly available through ESA's Planetary Science Archive. The OMEGA VNIR and SWIR-C channels data are co-registered according to Carrozzo et al. (2012). Together with CRISM, OMEGA allowed for the first time the clear detection of hydrated minerals such as hydroxides, sulphates and in particular phyllosilicates (e.g., Poulet et al., 2005; Gendrin et al., 2005; Arvidson et al., 2005; Milliken et al., 2008).

In order to investigate regions where hydrated minerals have been already found and to include a variety of mineralogical units, in this work we focus on the two MEx orbits: 0422_4 and 0353_3. Orbit 0422_4 includes the north of Syrtis Major Planum, passing through Nili Fossae and highlands

of Nili Fossae. This OMEGA observation contains 44,640 spectra and, besides the considerable mineralogical diversity, it shows significant variability in gas absorption due to an altimetry variation of 4.7 km. This observational session has been acquired on May 20th, 2004 during Martian year 27 (the Martian years start on 1955, April 11 at solar longitude 0°, following the convention used in Clancy et al, 2000), at solar longitude 36.1° (northern spring). The ground track goes from south to north crossing a changing elevation from -2.97 km to 1.73 km. Orbit 0353_3 passes through Mawrth Vallis, a region located at mid-low latitude in the west part of Arabia Terra, with an elevation spanning from a minimum of -5 km to a maximum of -700 m. This observational session has been acquired on April 30th, 2004 during Martian year 27, at solar longitude 26.8° (northern spring) and contains 99,820 spectra.

## 3. Method and validation

### 3.1 Principal component analysis and target transformation

This Section follows closely the methodology given in Bandfield et al. (2000). In statistical methods the covariance matrix is used, with different approaches, to derive the eigenvectors, a set of $N_e$ orthogonal spectral functions summarizing the variability of the sample. They can be organized in a $m \times N_e$ matrix $R$ ($m$ being the number of spectral points), whose rows can be linearly combined to reproduce every spectrum in the dataset. More specifically, being $D$ the full set of measured spectra ($n \times m$ matrix, gathering $n$ sampled spectra in $m$ spectral bands), it holds

$$D = R \cdot C \qquad (1)$$

where $C$ is a $N_e \times n$ matrix whose columns give the contribution (weights) of each endmember to the different spectra in the population. To derive the matrix $R$ (composed by eigenvectors of $D$) we use the PCA. However, there are many works that use instead the Factor Analysis (FA), such as Bandfield et al. (2000, 2002), D'Amore at al. (2013), Glotch and Bandfield (2006), Glotch and Rogers (2013), and Hamilton et al. (2012). PCA and FA have the same purpose: reduce the dimensionality of the variables. However, they reach this goal in two different ways: PCA uses the variance of the observed variables and finds the principal components, while FA accounts for common variance in the data and finds a smaller set of latent variables or scores (the original variables are defined as linear combinations of the factors). Both methods provide significant components (or eigenvectors) to be transformed in physically meaningful end-members by means the Target Transformation. In our opinion and for the goal of our work, both methods are useful in

the same way, and, we suppose, they could afford to achieve same or similar results. Therefore, we proceed using the PCA approach.

The main purpose of the PCA is to reduce the number of variables and found the minimum set of eigenvectors whose linear combinations are able to reconstruct the original measured spectra. The original population of spectra can be represented in a space with dimensionality given by the number of spectral channels. In the PCA approach, the diagonalization of the covariance matrix is used to represent the original information in a rotated space of reduced dimensionality, but preserving the most part of the original variance. Once the eigenvalues are sorted by decreasing values, the first eigenvector (principal component 1) accounts for the maximal variance, the second eigenvector (principal component 2), orthogonal to the previous one, accounts for the maximum variability that has not been counted from the first one, and so on. Once all eigenvalues and eigenvectors (their initial number is equal to the original dimension of data) have been found, the dimensionality can be reduced by retaining the minimum $N_e$ number of components that actually influence the dataset. Even if ideally $N_e$ should be strictly related to the number of spectral end-members present in the dataset, actually secondary eigenvectors could still contain spectral information. As explained in Section 3.2, we use a chi-square test to constrain the number of eigenvectors. The eigenvectors associated to the $N_e$ eigenvalues or principal components can thus reproduce the measured signal, while the remaining eigenvectors are featureless and contain mostly random noise.

Since the eigenvectors do not necessarily have a physical meaning, target transformation (Hopke, 1989) is used to assign a physical significance to this abstract matrix by rotating the space defined by the meaningful eigenvectors to be geometrically realigned to a set of predefined axes, called test vectors, representing the possible physical contributions to the measured data. For this purpose, a set of trial (or test) spectra have been computed by means of a radiative transfer (RT) code (Ignatiev et al., 2005), each one representing the gaseous spectral end-members: carbon dioxide, carbon monoxide and water vapour transmittances. The trial spectra describing the surface components can be laboratory spectra or retrieved surface components obtained with existing methods, e.g., the so called Mons Olympus' method (Langevin et al. 2005), hereafter MO method, which is also often referred as "volcano scan" (e.g., McGuire at al., 2009). The spectral components (R matrix in Formula 1) are then retrieved fitting the trial spectra with a linear combination of $N_e$ eigenvectors. Finally, the projection of the initial spectral population into the space defined by the retrieved spectral components allows finding the weight matrix (Hopke, 1989). Considering the retrieved end-members of the surface only, the gaseous components are removed from the spectra.

The assumption of linear combination of spectral end-members can be done only when the dust content in the atmosphere is very low, otherwise their contribution is far from being linear. Moreover, in the visible and near-infrared range of the spectrum it is difficult to disentangle the effect of dust on the bright, dusty terrains from that in the atmosphere. For this reason we will adopt a further step to remove the effect of atmospheric dust scattering, as described in Section 4.4. Therefore, in our first analysis the aerosol component is not included, and the assumed contribution to the spectra is only given by the gases transmittance and surface reflectance.

### 3.2 Synthetic datasets used as a test

To validate and check the accuracy of the described method we proceed with preliminary tests on simulated data and make a direct comparison between final results and initial input (which we call "true"). We consider a population of synthetic spectra computed by means of the RT algorithm and convolved with a Gaussian kernel at the OMEGA spectral resolution. The synthetic population has been constructed using the observational geometries of OMEGA orbit 0248_1 (16th pixel) that includes 2848 scans and shows an altimetry variation from -3.53 km to 1.96 km.

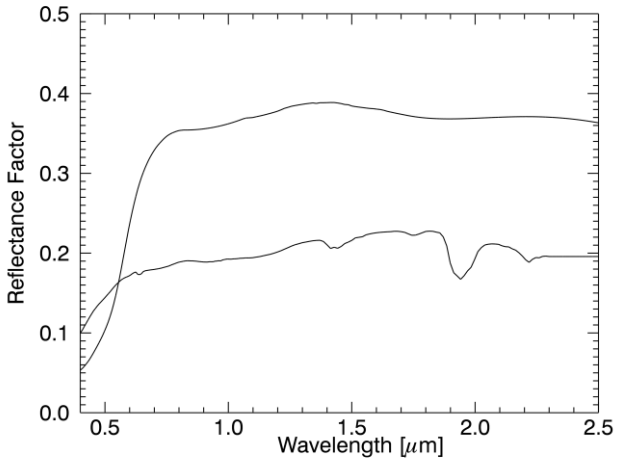


Figure 1. Reflectance of a bright surface (upper spectrum) and dark surface (lower spectrum) used as input for the surface reflectance in the RT code.

In the simulated dataset we consider a bright surface reflectance (in Figure 1, the upper curve) and a dark surface reflectance (the lower curve in Figure 1, taken from a spectrum of a hydrated mineral measured in laboratory). The two reflectances (Figure 1) are mixed with uniform random weights in each of the 2848 different spectra of the population and used as input for the surface reflectance in the RT code. The gaseous components include $CO_2$, CO and $H_2O$. Realistic gases abundances and pressure-temperature vertical profiles are extracted from the Mars Climate Database (MCD, Lewis

et al., 1999; Forget et al., 1999). Deep space measurements from OMEGA orbit 0285_0 have been used to derive the standard deviation of random instrumental radiometric noise. Series of normally distributed random numbers have eventually allowed us to simulate a realistic measurement error for each spectrum. Since the visible portion of the spectrum does not have gaseous absorption bands, this analysis involves the spectral range from 1 µm to 2.5 µm.

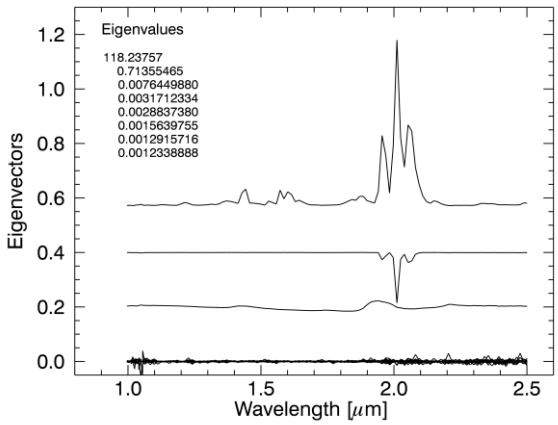


Figure 2. Eigenvectors retrieved using PCA for the simulated dataset, shifted for clarity. Only the first eight eigenvalues are listed.

The PCA applied to the synthetic population identifies a significant contribution of three principal components, which are found to be essentially the gases components (the first two eigenvectors) and the surface (the third eigenvector), as shown in Figure 2, whereas all the other eigenvectors contain mostly noise. However, the correct number of principal components, which represents the eigenvector space size, has been defined iteratively considering the best-fit value ($\chi^2=[\sum_{ij} (x_{ij} - y_{ij})/\sigma_{ij}^2]$/n_points, where *i* is the index on the spectra and *j* is the index on the spectral points, σ is the noise, x is the reconstructed spectrum, y is the original spectrum and n_points is the number of spectral points considered) between the reconstructed spectra and the initial spectra (Hopke, 1989), considering a signal to noise ratio of 100. Before PCA is performed, we cast the problem in the logarithm space, therefore multiplicative contributions become additive: this step extend the validity of eq. 1 to the solar-dominated region of the spectrum. Then we remove the mean that obviously is equivalent to a ratio of each spectrum by the average. Then the mean is included as an additional component. However, it is not necessary to remove the mean before the analysis is performed. Indeed, the retrieved spectral components are quite the same in both cases.

Based on the method described above, we compute the surface components for the simulated population. Figures 3a and 3b show the result of target transformation applied to the gas and surface components, respectively.

The retrieved gas spectral end-member (red line in Figure 3a), in addition to the strong $CO_2$ absorptions, shows the contribution of CO and $H_2O$ (e.g., absorptions at about 1.35 µm and 1.9 µm for $H_2O$ and at about 2.3 µm for the CO) even if they have not been included in the trial spectrum, showing the ability of the method to recognize spectral signatures even if not present in the trial spectrum. Figure 3b shows that the TT is able to infer the correct shape of the surface spectral end-member (red line).

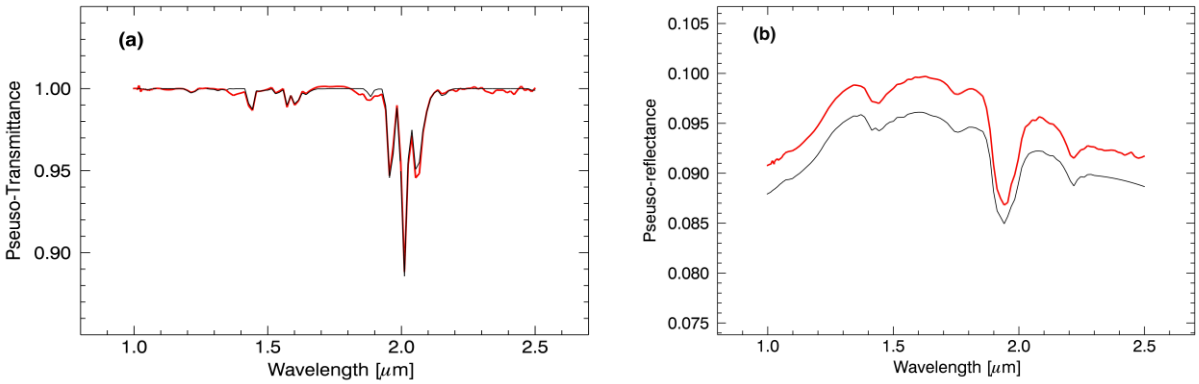


Figure 3. (a) Gas spectral component (red line) retrieved by fitting the trial spectra (black line) with a linear combination of significant eigenvectors. The gas trial spectrum (black line) is a simulated spectrum, which considers the contribution of carbon dioxide only. (b) Surface spectral component (red line, shifted for clarity) defined as the best-fit representation of trial spectrum (black line) with a linear combination of significant eigenvectors. The trial spectrum for the surface component (black line) is the linear combination of the dark and bright surface reflectance shown in Figure 1.

Once the weights of each spectral component have been computed for every spectrum of the population, the surface reflectance is retrieved. The residuals (Figure 4) show the percentage error of the method and it is computed as the difference between the true surface and the retrieved surface normalized to the true surface. The error is less than 1% except in few spectral points where it reaches values of about 2%.

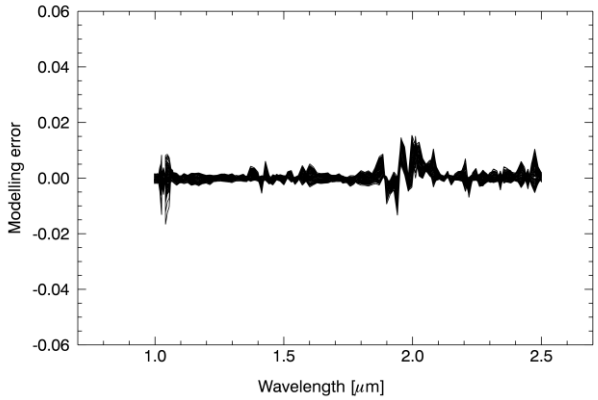


Figure 4. Modelling error computed as the difference between the true surface and the retrieved surface normalized to the true surface.

Figure 5 shows the retrieved surface components (red spectra) for two spectra of the population. The method, described in the present work, permits a successful reconstruction of the surface reflectance (being the residual errors less than 2%) and of the spectrum (Figure 6). We check also if the elevation variability is necessary for the application of the method. Therefore, we consider a simulated population where the atmospheric path length is uniform and only the surface spectra are variable. The method works very well even in this case, showing almost the same residuals of Figure 4. Indeed, we still have a variability that makes the PCA working fine.

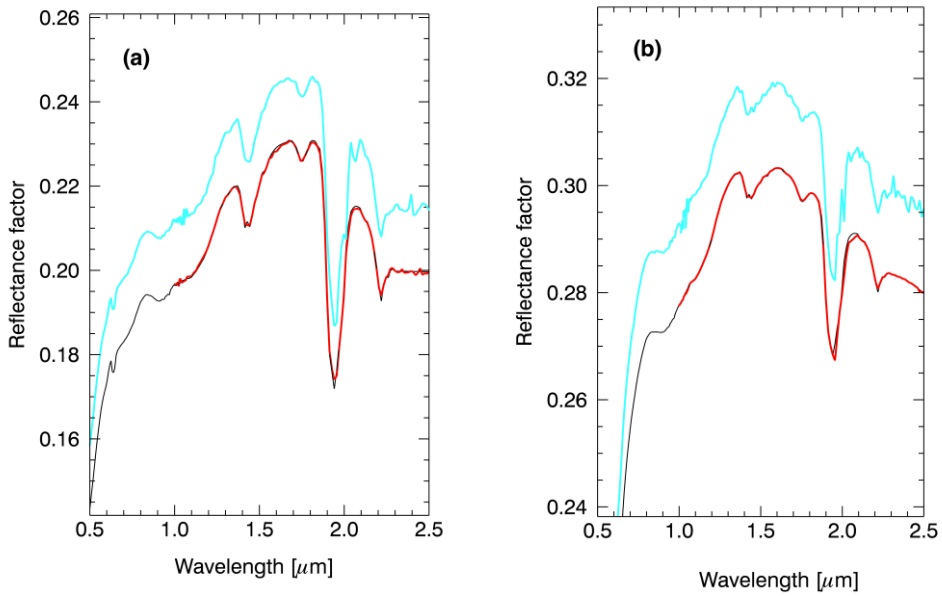


Figure 5. (a) Spectrum whose surface reflectance is made by 1% of bright component and 99% of dark component. (b) Spectrum whose surface reflectance is made by 50% of dark component and 50% of bright component. The retrieved surface reflectances are the red line over imposed to the true surface reflectance (black line). Shifted for clarity the

surface reflectance obtained with the MO method (cyan line).

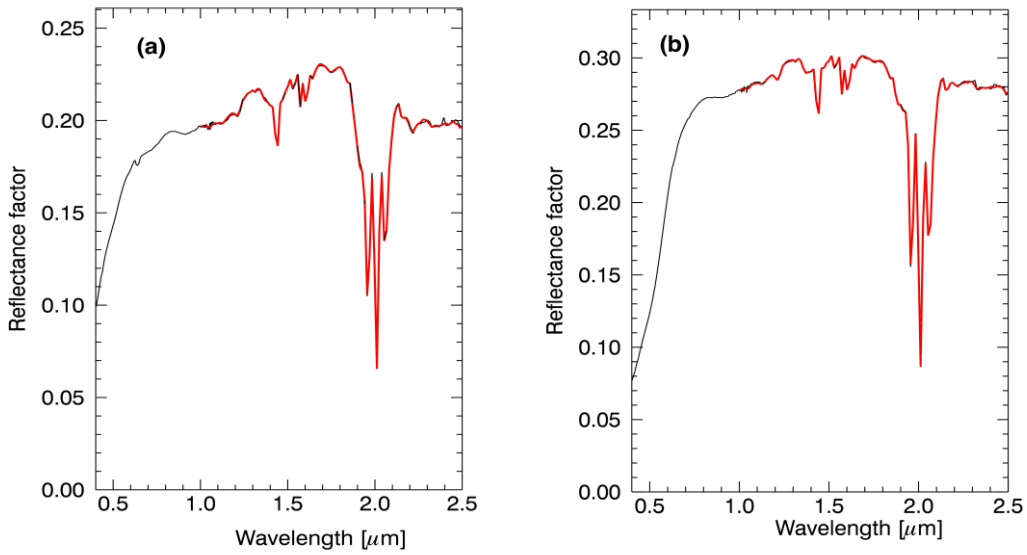


Figure 6. Reconstructed spectrum (red line) compared to the initial population (black line) for the same cases of Figure 5.

## 4. Application to the OMEGA data

### 4.1 Trials and first guess discussion

We have applied the procedure described in Section 3 to OMEGA cubes 0422_4 and 0353_3, covering Nili Fossae and Mawrth Vallis, respectively. The application of the PCA to both datasets reveals that five eigenvectors (Figure 7a and 7b, for cube 0422_4 and 0353_3, respectively) have a spectral shape above the noise, meaning that at least five components mostly influence the dataset. We apply the same procedure described in Section 3.2 and chose as trial spectra for the surface the reflectance obtained using the MO method, while the gas components are the same used for the test case with a correction at 2.039 μm because of a bad spectel (Forget et al, 2007). By using the already existing spectral shape for the surface end-member as a first guess in the SAS analysis we can reach meaningful solution for every spectrum in the analyzed dataset. In fact, the MO method provides a surface reflectance that at first order well represent the mineralogical diversity as reported in the OMEGA and CRISM data analysis literature and in the derived spectral indexes used to map on a global scale the different class of minerals found on Mars (eg. Poulet et al., 2008; Pelkey et al., 2007; Carrozzo et al., 2012; Ody et al., 2012).

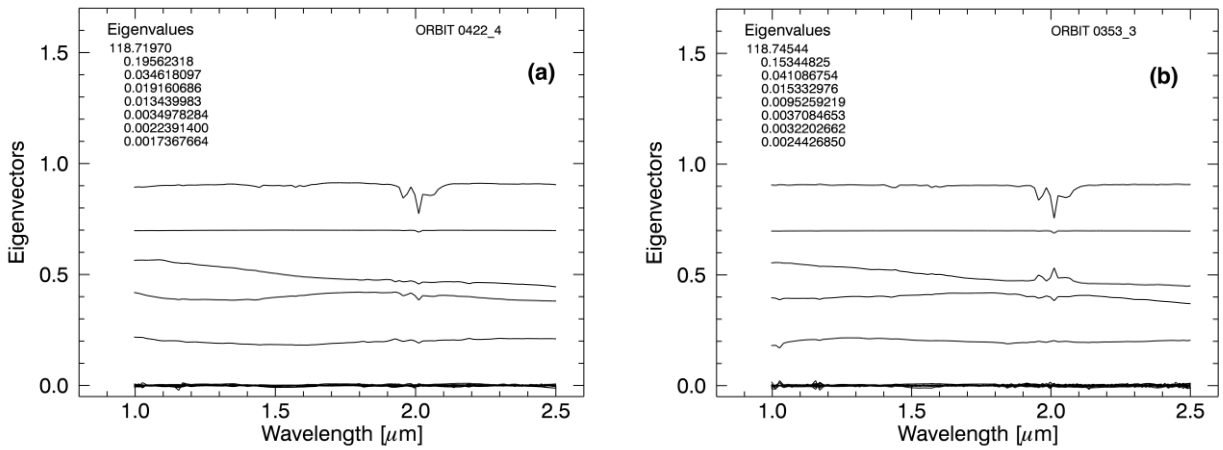


Figure 7. Eigenvectors (shifted for clarity) retrieved using PCA for the two considered orbits. Only the first eight eigenvalues are listed.

## 4.2 Nili Fossae, orbit 0422_4

The eigenvectors obtained after the PCA has been applied to the spectral population of orbit 0422_4 clearly indicate that the principal components that influence this dataset are characterized by gaseous spectral features and surface spectral shape (Figures 7a). As described in the test case, we consider a number of eigenvectors that gives the best reconstruction of the spectra when compared (by means of the chi-square test) with the original spectra measured by OMEGA. This ensures that we are observing the best combination of the retrieved end-members. Figure 8a shows the retrieved gas spectral components and their amplitude in the dataset. This is possible using the retrieved weights (C matrix in Formula 1) obtained by projecting the spectral population in the space defined by the retrieved end-members. The weights of the gas spectral components multiplied to the gas end-member give the gases opacities, since we are working in the logarithm space. Target transformation projection of surface trials in the space defined by the eigenvectors and the resulting best fit of the linear combination of the selected eigenvectors with the trial component is plotted in Figure 8b for a spectrum where the hydrated band is present.

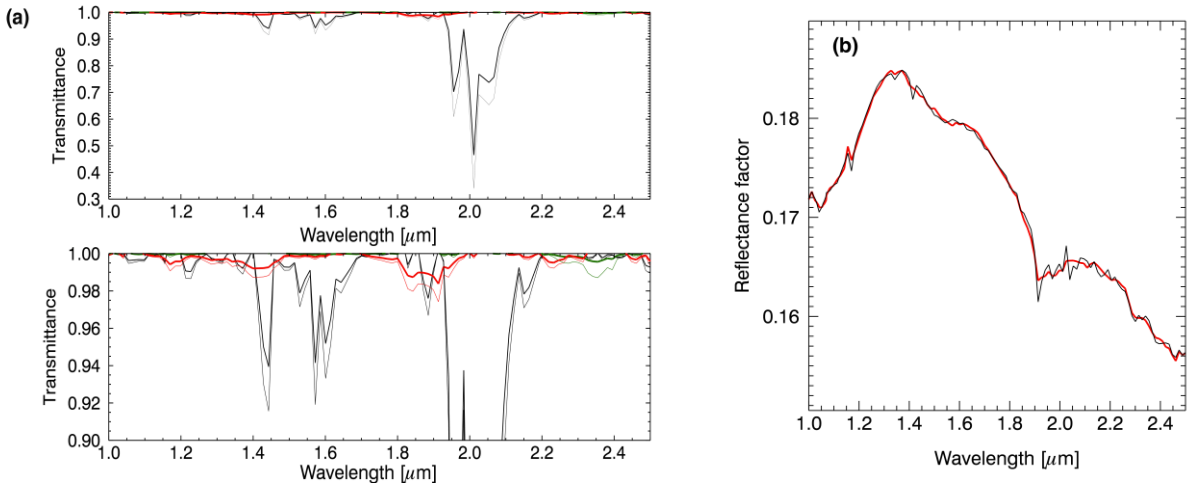


Figure 8. (a) Retrieved transmittances corresponding to the maximum (thick line) and minimum (thin line) weights. The $CO_2$ transmittances are the black lines, the $H_2O$ transmittances are the red lines and the CO transmittances are the green lines. The lower panel is a widening of the upper panel to have a better viewing of the CO and $H_2O$ transmittances. (b) Surface trial (black line) and retrieved surface end-member (red line) for a case where the hydrated band is present.

Figure 9 displays the retrieved surface reflectance for bright and dark surfaces from cube 0422_4. The surface reflectances obtained using SAS procedure are similar to the ones retrieved with MO method, but a reduced noise and a better evaluation of the spectral shape of the surface are obtained in the spectral region where the gaseous component is stronger, in particular around 2 µm.

In Nili Fossae region the 2.3 µm band has been detected (e.g., Poulet et al., 2005; Mangold et al., 2007; Mustard et al., 2007; Michalski et al., 2010) in association with the hydration band at 1.9 µm. This combination of absorptions was attributed to Fe/Mg-rich clays. Figure 10a shows one of these peculiar spectra as an example of the result obtained by the application of the SAS procedure to a surface spectrum characterized by phyllosilicates features. In some cases we also observe a shift in the minimum of the band at 1.9 µm (see one case in Figure 10b, red line). This shift consists of one spectral point compared with the spectra of surface obtained with MO method (black line). In order to make a deeper check on this result, we search for spectra of surface in the same region of Mars using the dataset of CRISM/MRO instrument. Figure 10b shows a spectrum (blue line) from CRISM instrument (on the same spatial region, even if CRISM spectrum is obtained at much higher spatial resolution than OMEGA spectrum) where the position of the 1.9 µm band coincides with that of our retrieved surface reflectance.

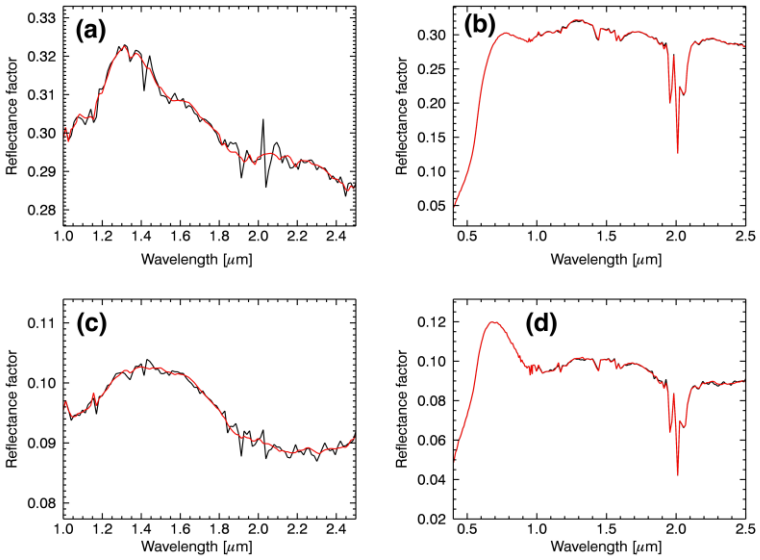


343

344 Figure 9. Spectra from orbit 0422_4 crossing bright and dark surfaces. (a and c) Surface reflectance factor retrieved
345 using the methodology described in the paper (red spectra) overlying to surface reflectance obtained using MO method
346 (black spectra). (b and d) Original OMEGA spectra (black line) underlying the retrieved spectra (red line) using the
347 SAS procedure (red line).

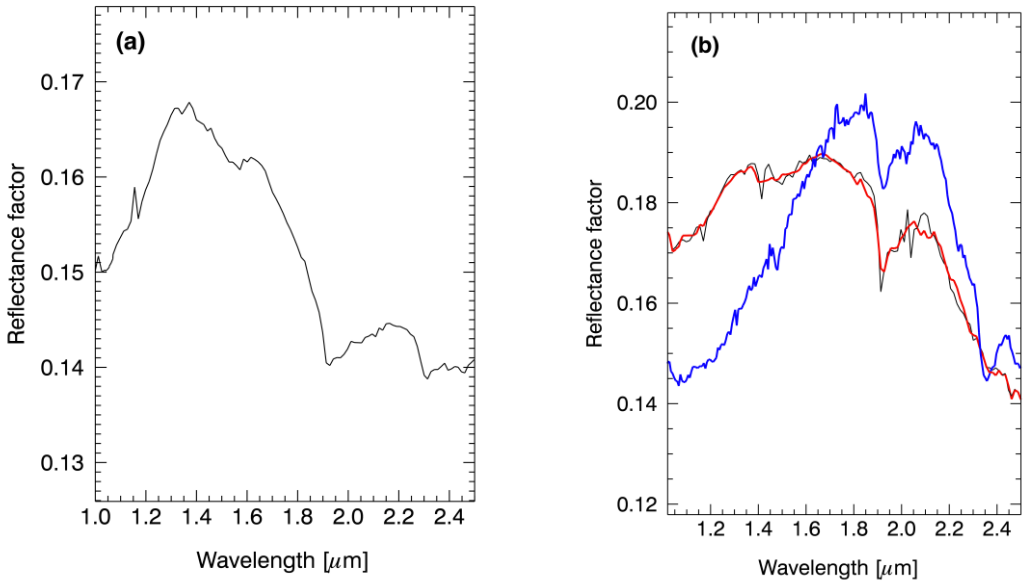


348

349 Figure 10. (a) Surface reflectance from orbit 0422_4 showing the absorption at 1.9 µm associated to 2.3 µm band
350 indicating Fe/Mg-rich clays. (b) Surface reflectance factor showing the spectral feature of hydrated minerals at 1.9 µm,
351 2.3 µm and 1.4 µm in Nili Fossae region of Mars (MEX orbit 0422_4). The red line is the surface reflectance retrieved
352 with the SAS procedure, the black line is the surface reflectance obtained with MO method, and the blue line is a
353 CRISM observation of the same region but with a higher spatial resolution. The SAS method has not been applied to the
354 CRISM spectrum in the figure, but the atmospheric features have been removed with "volcano scan" method (McGuire
355 at al., 2009).

### 4.3 – Mawrth Vallis, orbit 0353_3

In this session we present and discuss the results of the SAS procedure to the OMEGA spectra from orbit 0353_3. Figure 7b shows that the principal components obtained with the PCA have the typical features of the gas and surface shape. The application of target transformation can be seen in Figure 11. The reconstructed spectra with the SAS method are indistinguishable from the original spectra except for the noise that is reduced after the application of SAS method. The absorption at 1.9 µm is present in many regions of the area as shown in the map of Figure 12a, where the violet colour indicates spatial regions where the spectral index values of 1.9 µm band (as defined in Loizeau et al., 2007) derived from the retrieved surface, are higher than 2.5%. We consider an average of nine surface spectra (the average should remove random noise), from both the MO and SAS methods, located in the region of the map indicated with a red box. These spectra are all characterized by hydrated mineral features and their average is shown in Figure 12b with cyan and red colours for MO and SAS method, respectively. To remove residuals due to atmospheric gases, the ratio with a featureless surface reflectance measured in a region (yellow box in Figure 12a) very near to the selected area has been considered and shown as green and black coloured spectra in Figure 12b for MO and SAS method, respectively. The spectrum retrieved with our statistical analysis shows clearly the main hydrated features if compared with the spectrum of nontronite (violet line) taken from the USGS mineral spectral library (Clark et al., 1993) and does not differ substantially from the normalized spectra.

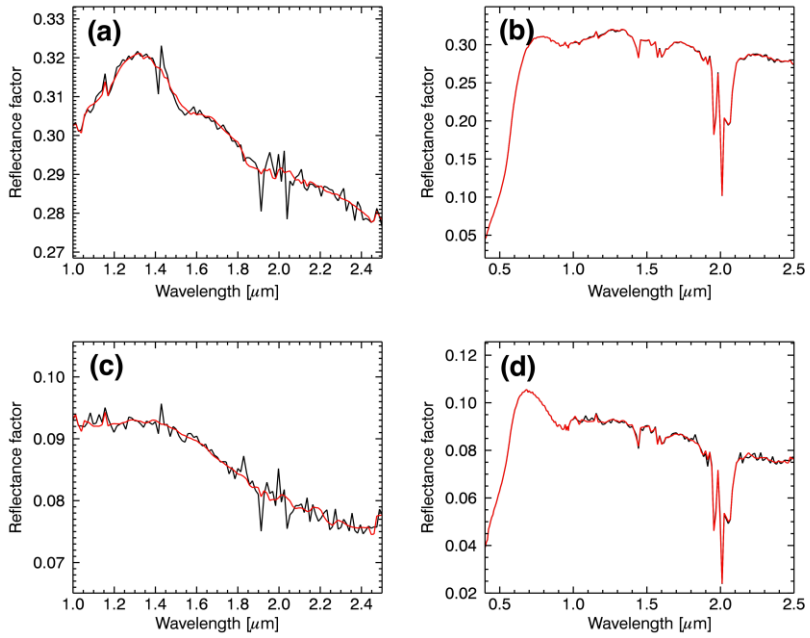

Figure 11. Spectra from orbit 0353_3 crossing bright and dark surfaces. (a and c) Surface reflectance factor retrieved using the methodology described in the paper (red spectra) overlying to surface reflectance obtained using MO method (black line). (b and d) Original OMEGA spectra (black line) underlying our retrieved spectra (red line).

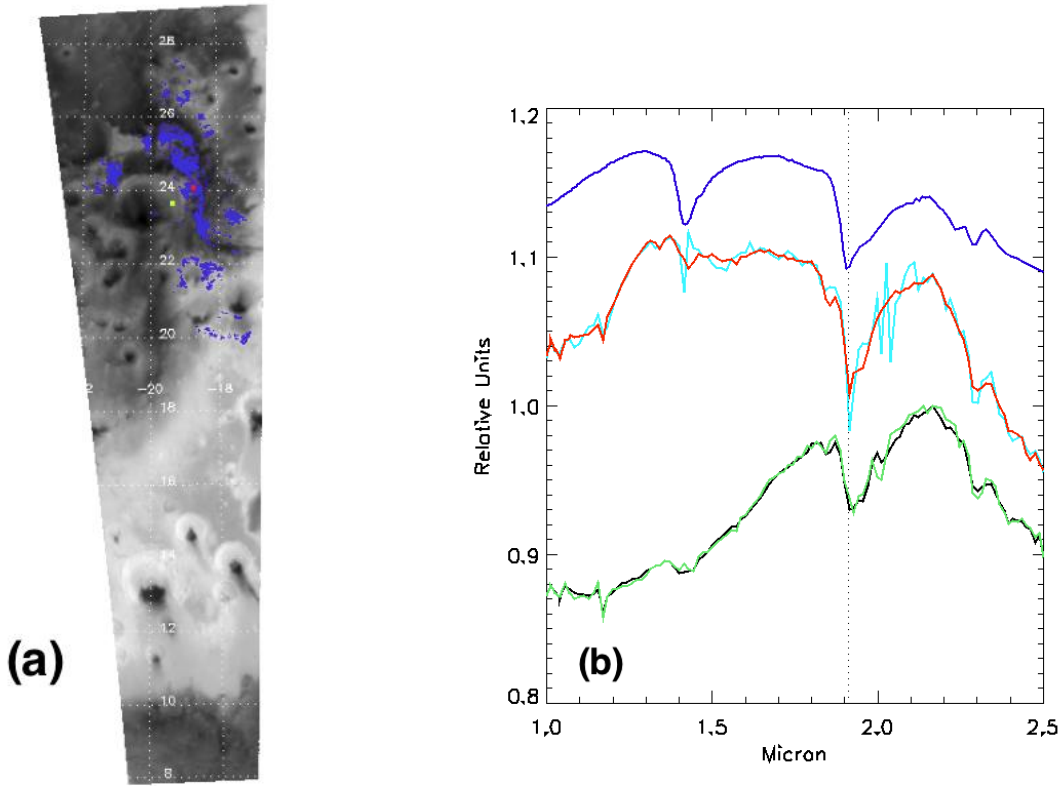


Figure 12. (a) The violet area is characterized by a band depth at 1.9 µm higher than 2.5% (as derived from the retrieved surface) overlying the albedo map at 1 µm of orbit 0353_3. (b) The violet spectrum is a laboratory spectrum of nontronite, red and cyan spectra are surface reflectance (normalized at 1.4 µm and shifted for clarity) obtained with the SAS and MO analysis respectively and corresponding to the region indicated with a red box in the map. Green and black lines are surface reflectances measured around the pixel indicated with the red box and rationed with a featureless spectrum measured in the region indicated with a yellow box in the map, considering the MO and SAS method respectively.

### 4.4 Correction for the effect of atmospheric dust

Dust is always and everywhere present in the Martian atmosphere showing opacity variation with season and location as described in Smith (2004). Mars experiences global dust storms as well as local dust storms and small-scale dust devils. Uplifted dust strongly influences the thermal structure of the atmosphere. During the observational session of orbit 0442_4 the dust optical depth $\tau$ (at 1070 $cm^{-1}$) ranges from 0.1 to 0.2, as reported in MCD and shown in Figure 13a. The dust optical

depth is slightly higher for orbit 0353_3 (Figure 13b), especially in the atmospheric column above craters south of 16° of latitude, where τ can be greater than 0.25. We extract the value of dust optical depth from MCD to have the value of τ influencing each spectrum. The dust input scenario is the one called "Mars Year 24" (MY24) designed to mimic Mars as observed by Mars Global Surveyor from 1999 to 2001, a Martian year thought to be typical (MCD, user manual). Vincendon et al. (2007) used a Monte Carlo approach to determine both the aerosol thickness and the surface reflectance factor free from the aerosol contribution at each wavelength in OMEGA near-infrared spectra for high-latitude regions of Mars. We apply the same approach from visible to near-infrared spectral range (from 0.4 µm to 2.5 µm) considering that the observed reflectance factor at a given wavelength is a function of surface reflectance and τ. Taking advantage of this relationship and knowing τ a priori, we use a multiple-scattering radiative transfer code to simulate reflectance factor, assuming the most recent properties for the atmospheric dust (Wolff et al., 2009) and using the observing geometries for each observation. The grain size distribution of dust is described with a log-normal function where the grain effective radius is 1.6 µm and the effective variance of distribution is 0.35 µm. The surface reflectance factor is determined as the value that corresponds to the best fit between the observed reflectance factor and the simulated one for each wavelength.

The effect of the dust on the spectra depends on the surface reflectance. For dark surfaces the effect of dust is to increase the reflectance while, on contrary, for bright surfaces is to decrease the reflectance. For intermediate values of surface reflectance the effect of atmospheric dust is not distinguishable from that of surface dust. These effects are shown in Figure 14 where two spectra from orbit 0422_4 and two from orbit 0353_3 corrected for the effect of dust are plotted. The displayed surface reflectance shows how the effect of dust can be different for bright (Figure 14a, orbit 0422_4) and dark (Figure 14c, orbit 0353_3) surfaces and how the presence of atmospheric dust cannot be distinguished for intermediate values of surface reflectance (around 0.2, Figure 14b and 14d for orbit 0422_4 and 0353_3, respectively). It is also evident that the narrow spectral features of the surface are not modified by the effect of dust due to scattering, while the continuum is influenced by the dust contribution.

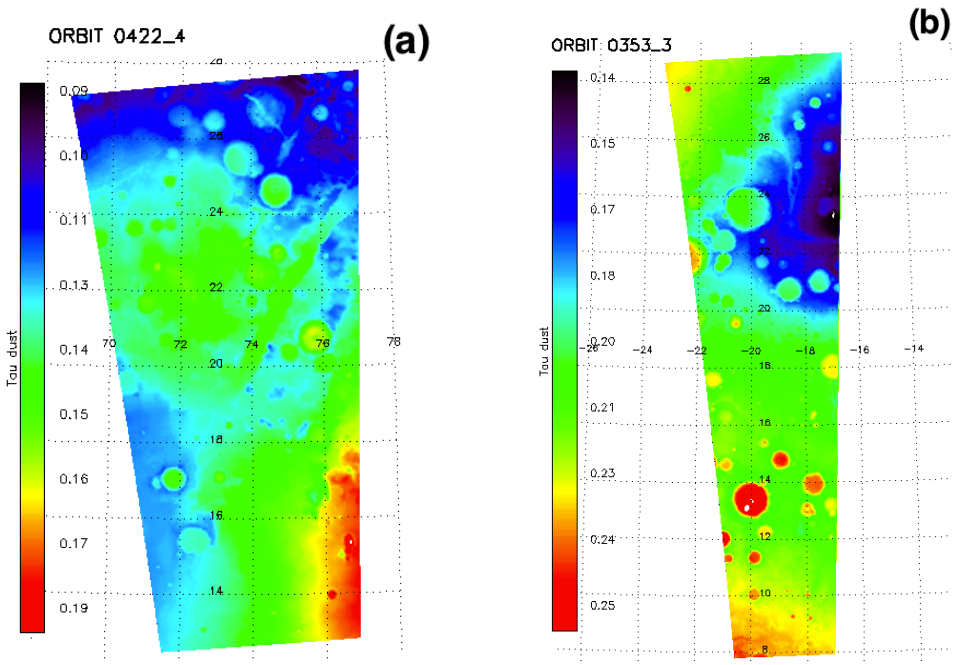


Figure 13. Maps of dust optical depth (at 1070 $cm^{-1}$) as extracted from MCD. (a) Orbit 0422_4 and (b) orbit 0353_3.

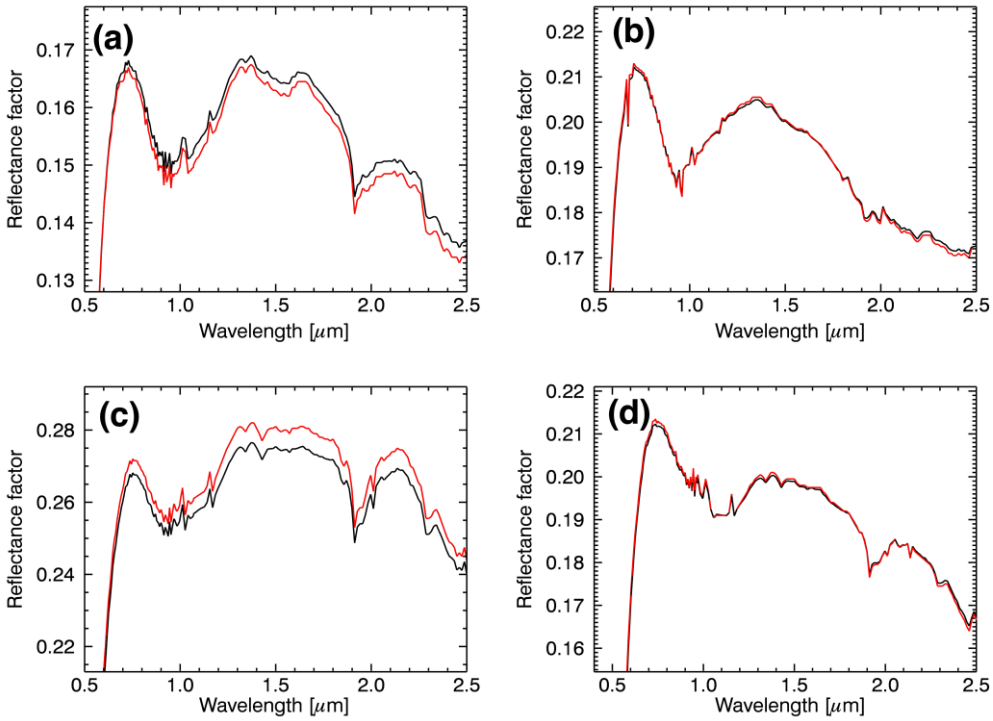


Figure 14. (a) Orbit 0422_4: pixel 75, scan 152. (b) Orbit 0422_4: pixel 77, scan 111. (c) Orbit 0353_3: pixel 41, scan 582. (d) Orbit 0353_3: pixel 38, scan 538. The black line is the surface reflectance and the red line is the surface reflectance corrected for the effect of dust in the atmosphere. The dust optical depths are 0.137 and 0.138 and 0.217 and 0.172 for the shown spectra of orbit 0422_4 and 0353_3, respectively.

## 5. Application of MGM analysis to Martian surface spectra

Removing the atmospheric contribution in the Martian VNIR-IR spectra is crucial to study and map the surface mineralogy from remote sensing data. In this Section we discuss how the Martian surface spectra retrieved by means of the SAS method can be used to study in details the mineralogy of Martian surface, with particular attention to hydrated phases. We spectrally analyse the two OMEGA cubes, from Nili Fossae and Mawrth Vallis, focusing on the retrieving of the Martian mineralogy by using the MGM (Sunshine et al., 1990). In particular, we focus our analysis on those minerals characterized by absorption bands centered at 1.9 µm to 2.3 µm, representative of hydrated minerals, in which spectral range the atmospheric contribution is more important. In order to validate the surface spectra obtained through the SAS method, we apply the MGM deconvolution to both a set of laboratory spectra of minerals of recognized hydrated silicates on Nili Fossae and Mawrth Vallis and to the SAS OMEGA spectra.

The MGM is a statistic-base method based on the assumption that different mineral absorptions can be described with a modified Gaussian distribution superimposed on to a continuum. It is widely applied on mineral phases and mixtures analysis, in particular for the electronic absorptions (e.g., Sunshine et al., 1990; Sunshine and Pieters, 1993, 1998; Klima et al., 2007, 2011; Clenet et al. 2011; Serventi et al., 2014submitted). Different papers used also Gaussians models to determine the vibrational overtones present in hydrated silicates, carbonates and sulfates measured in laboratories (see Sgavetti et al., 2015; and references therein). Mustard et al. (2005) showed how pyroxene-rich areas on Mars have wide absorptions at 1 and 2 µm on OMEGA data and how applying the MGM it is possible to separate orthopyroxene from clinopyroxene contribution. Recently, Clenet et al. (2013) applied the MGM to OMEGA data exploring the mafic mineralogy of Syrtis Major. The authors highlighted how the application of MGM on OMEGA data permits to separate the different contribution of mafic minerals and to quantify their parameters.

Here, we apply the MGM considering:

1) the continuum as a straight line as function of the wavenumber, with two parameters, the offset and the slope (Sunshine et al., 1990);
2) each Gaussian is described by three parameters: the band depth (in logarithm of the reflectance), the band center and the band width, or FWHM (both in nanometers).

We choose a continuum that model the real strength of the absorption bands (see also Clenet et al., 2011) thus avoiding an horizontal continuum by choosing a fixed, tangent continuum. On the other hand, Gaussians spectral parameters are free to vary. The goodness of the fit is expressed by the RMS (root mean square) value.

466 We select spectra of some clay minerals (e.g., nontronite and smectite) from USGS spectral library
467 (Figure 15 and Table 1), which can be considered analogues to Martian phases. Taking into account
468 the literature, which discusses the mineralogy of the selected regions, we consider nontronites,
469 smectites and montmorillonites as laboratory hydrated phases. These minerals belong to the
470 smectite family, already recognized on Martian surface, as in Nili Fossae (Ehlmann et al., 2008) and
471 are characterized by absorption bands comparable with spectra here analysed. Electronic
472 absorptions characterize the 0.5-1.2 μm spectral region and, in particular, bands centered between
473 0.8 and 1.2 μm are due to $Fe^{2+}$ transitions. On the other hand, overtones and combination of modes
474 characterize the longest wavelength. In particular, smectite, nontronite and montomorillonite have
475 the strongest water overtones near 1.41 μm and water combination bands near 1.92 μm. As shown
476 in Ehlmann et al. (2008; and references therein) the absorption at 1.4 μm (due to the OH stretching)
477 depends on the octahedral cations present in crystal structure of hydrated minerals. The stretching
478 occurs at 1.43 μm, at 1.41 μm and at 1.38-1.39 μm if the cation is Fe, Al or Mg, respectively. H-O-
479 H combination stretching and bending vibrations occur near 1.92 μm and 1.97 μm, respectively
480 (Bishop et al., 2008). Weak combination bands have been detected at 2.0 μm for adsorbed water in
481 hydrated minerals. Strong OH combination bands are also present in the 2.2-2.5 μm spectral region,
482 and, as the 1.4 μm absorption, their position is a function of the octahedral cation composition. In
483 general, the OH combination bands occur at 2.17-2.21 μm, 2.29-2.31 μm and 2.32-2.34 μm if Al,
484 $Fe^{3+}$ and Mg are in the octahedral sites, respectively. Al/Fe-OH combination bands occur at 2.24
485 μm. If the cation is the $Fe^{2+}$ the band is centered at 2.35-2.37 μm. Bishop et al. (2002a) interpreted
486 the additional bands between 2.4 μm and 2.5 μm as due to further OH stretching and bending.
487 Bands at 1.6-1.8 μm have not been recognized in the literature, and they can be due to the
488 continuum-removal applied in our deconvolution.

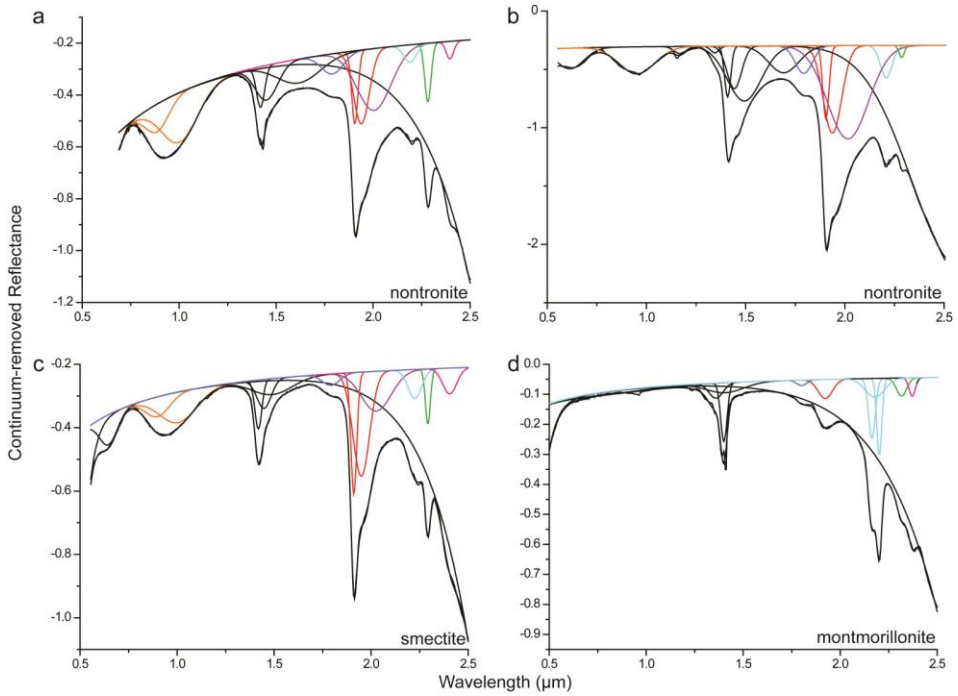


Fig. 15 MGM deconvolution on laboratory hydrated minerals: a,b) nontronites; c) smectite; d) montmorillonite. Spectra selected from the USGS spectral library are the black lines; the absorption contributions obtained with the MGM deconvolution are shown with colored lines.

As a result we can clearly determine the different absorption contributions on overtone and their combinations, and differentiate the various phases bearing to the clay minerals by considering the position of Modified Gaussians.

The same MGM approach is also applied on OMEGA surface spectra of the two considered orbits where hydrated phases where recognized, as derived by both the MO method and the SAS one. Results are shown in Figure 16 and summarized in Table 1. We find that:

a) very few differences are present in the 0.5-1.4 μm spectral region, comparing spectra after application of MO or SAS;
b) in the NIR range, spectra processed with the SAS method allows to recognized more absorptions within the composite bands and, therefore, an higher number of Gaussians is requested with respect to the MO method, likewise for the laboratory spectra dataset.

The main differences are in the 1.9-2.1 μm spectral region. In the MO surface spectra, the absorption bands are described with only two or three Gaussians despite the higher Gaussian number used for hydrated minerals, and residuals due to atmospheric contribution are high. On the contrary, in spectra corrected with SAS method, the same spectral region can be described with five/six Gaussians with a slight variation in position and depth, better fitting the overtone

absorptions and revealing differences in hydrated mineralogy or in their abundance. Moreover, spectral residual is five times lower.

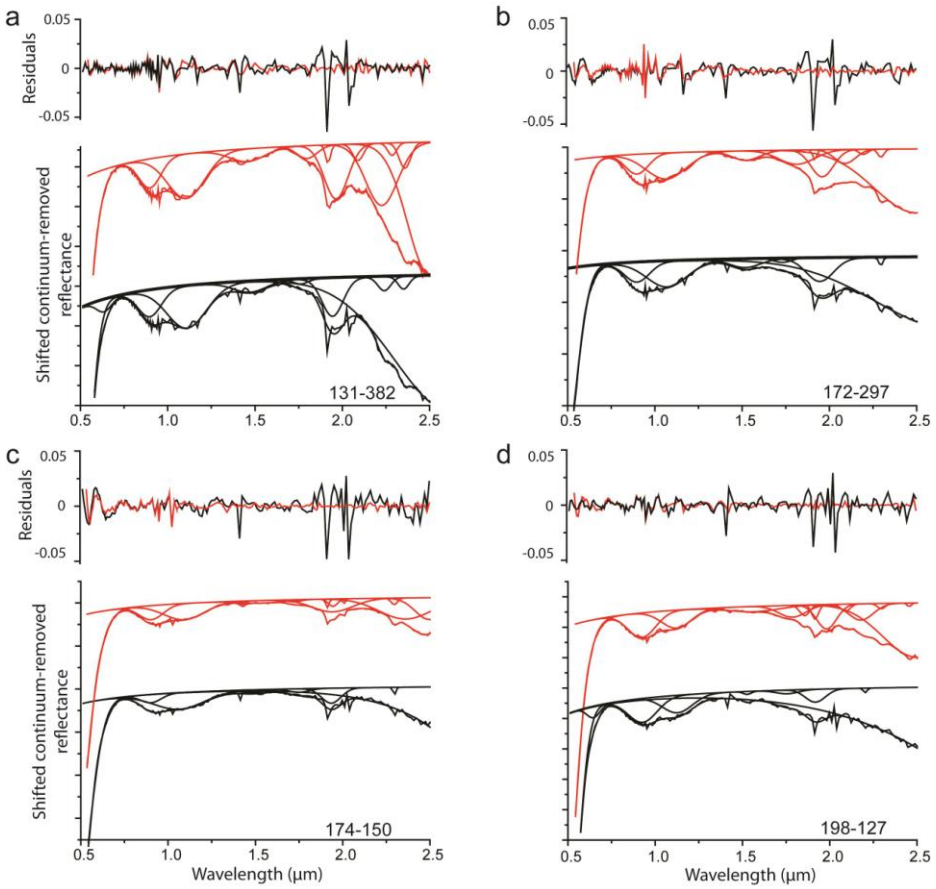


Figure 16 Figure shows Gaussians and residuals after MGM deconvolution. Black: spectra acquired from images after MO; red: spectra acquired from images after SAS. a,b : Nili Fossae; c,d: Mawrth Vallis.

It is clear that MGM on laboratory minerals shows deeper bands, explainable with different reasons, such as different particle sizes, presence of darkening agents and mixing effects on a planetary surface, etc.

The band centers obtained for the spectra after the SAS correction are comparable with those obtained from laboratory spectra. This indicates that hydrated mineralogy can be evidenced by applying MGM on spectra corrected by SAS, and we have seen that the selected spectra are comparable with the composition indicated in the literature (Ehlmann et al., 2008, 2009; Poulet et al., 2008). Moreover we can model the different absorption processes of these spectra. This aspect allows to better quantify and separate the possible different clay phases. Differences of few

nanometers can be due either to a mix of hydrated minerals in the analysed regions or to a slightly different composition.

On the contrary, the lesser number of Gaussians recognized in spectra after MO correction can lead to difficulties in mineralogical interpretation after MGM deconvolution. In fact, the wider Gaussians resulting in the spectra after MO correction (Figure 16) do not permit to separate and to recognize all the vibrational contributions present in the overtone bands, as expected from the analysis of laboratory data (Figure 15).

In conclusion, by decreasing the level of both the atmospheric residuals and random noise in the OMEGA data when retrieving the surface component, SAS method enable us to improve the investigation of hydrated mineralogy present in Nili Fossae and Mawrth Vallis by means of MGM. A higher number of Gaussians can be considered with respect to the previous technique in the 1.8-2.1 µm spectral range and a better comparison with laboratory data is reached.

| 131-382 | | 172-297 | | 174-150 | | 198-127 | | Nontronite | Nontronite 2 | Smectite | montmorillonite | Interpretation |
|---|---|---|---|---|---|---|---|---|---|---|---|---|
| MO | SAS | MO | SAS | MO | SAS | MO | SAS | | | | | |
| 0.896 | 0.898 | 0.897 | 0.897 | 0.902 | 0.904 | 0.928 | 0.923 | 0.887 | 0.9519 | 0.900 | 0.951 | $Fe^{2+}$ |
| 1.109 | 1.106 | 1.07 | 1.064 | 1.063 | 1.092 | 1.128 | 1.122 | 1.003 | | 1.005 | | |
| 1.470 | 1.455 | 1.518 | 1.522 | 1.485 | 1.427 | 1.527 | 1.568 | 1.42 | 1.409 | 1.419 | 1.364 | $OH^-$ |
| | | | | | | | | 1.45 | 1.443 | 1.448 | 1.392 | |
| | | | | | 1.537 | | | | 1.496 | 1.491 | 1.401 | |
| | | | | | | | | 1.617 | 1.692 | | | |
| 1.762 | 1.798 | 1.732 | | 1.751 | 1.723 | 1.757 | 1.786 | 1.798 | 1.793 | 1.793 | | |
| | | | 1.813 | | | | 1.857 | | | | 1.804 | |
| | 1.918 | | 1.916 | | 1.913 | | | 1.906 | 1.904 | 1.911 | 1.922 | $OH^-$ |
| 1.944 | 1.965 | 1.946 | 1.959 | 1.935 | 1.943 | 1.918 | 1.916 | 1.94 | 1.937 | 1.95 | | |
| | | | | | 1.945 | | 1.982 | | | | | |
| | 2.09 | | 2.09 | | 2.005 | | 2.09 | 2.005 | 2.015 | 2.027 | | |
| | | | 2.194 | | | | 2.179 | 2.19 | | | 2.164 | Al-OH |
| 2.241 | 2.226 | | | | | 2.203 | | | 2.209 | 2.226 | 2.203 | |
| | 2.285 | 2.294 | 2.295 | 2.297 | 2.296 | | 2.296 | 2.282 | 2.286 | 2.293 | 2.317 | Fe/Mg-OH |
| 2.351 | 2.359 | | | | 2.362 | | | 2.396 | | | 2.373 | |

Table. 1 Band centers found by the MGM deconvolution.

## 6. – SAS method applications

By completely separating the atmospheric component from the surface one, the results obtained with the method described in this work have many scientific implications for the study of the Martian orbiter data in the infrared spectral range:

- Since each gas spectral end-member can be isolated and their opacities can be estimated by means the TT, it is possible to retrieve the geographical distribution of the gaseous components. In particular the opacities distribution as well as the gaseous column density

(if a uniform mixing is assumed with altitude in the atmosphere and the absorption coefficients are known) can be determined.

- The final surface spectra we are able to obtain are of great importance, for example, in the study of ice clouds where the knowledge of each spectral component (including the dust contribution to the spectra) is crucial to estimate the ice properties.
- The spectral index maps can be greatly improved, especially for weak mineralogical absorption bands. In Figures 17a and 17b we compare our spectral index maps with those obtained with MO method. We consider orbit 0353_3 (Mawrth Vallis) and spectral index maps at 1.93 µm and 2.3 µm. The comparison shows that, for the 1.93 µm spectral index maps, the two methods give the same results, while at 2.3 µm the map obtained with SAS method is considerably improved respect to the one obtained with MO method.
- Usually, in order to minimize the MO atmospheric residuals and retrieve a smoother surface relative component to be compared with mineral spectral libraries, the analysis of OMEGA and CRISM spectra requires the ratio with a featureless surface reflectance measured in a region very near to the selected area. Hydrated mineralogical features in the OMEGA surface reflectance spectra retrieved by SAS (in particular in the 1.8-2.1 µm range) show a better consistency with laboratory data, without necessary rationing the data. The SAS surface reflectance spectra can be used to deconvolve the contribution of different minerals in the data, not only those highlighted by the rationing.
- The lower level of the atmospheric and noise residuals in the retrieved surface reflectances with SAS method enables us to make a better match with the MGM deconvolution parameters found for the laboratory spectra of Martian hydrated mineral analogues, allowing a deeper investigation of this spectral range.

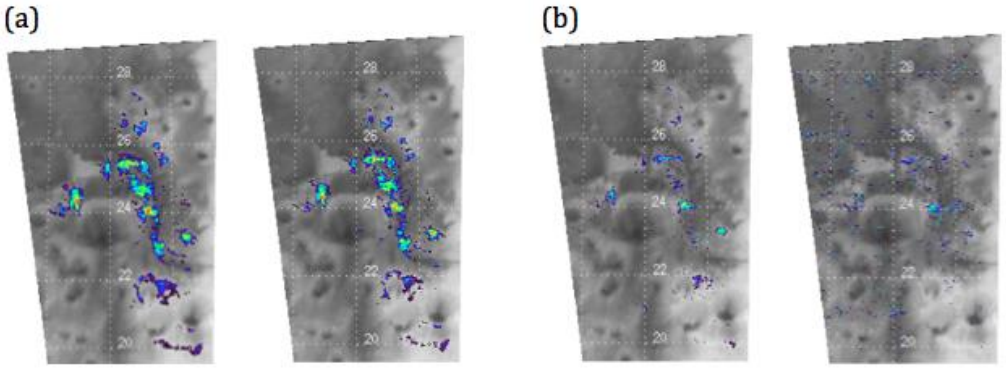


Figure 17: (a) Albedo map at 1 µm superimposed with the spectral index maps of the 1.93 µm band obtained considering surface reflectance with SAS method (on the left, using as threshold the 3σ of Gaussian distribution of values) and with MO method (on the right, considering a detection threshold of 2%). (b) Albedo map superimposed with spectral index maps of the 2.3 µm band obtained considering surface reflectances with SAS method (on the left,

using as threshold the 3σ of Gaussian distribution of values) and with MO method (on the right, considering a detection threshold of 2%).

## 7. – Conclusion

The removal of atmospheric contribution from reflectance spectra measured by airborne instruments is crucial to investigate the features of the surface, which are on the same spectral regions of atmospheric components. In particular, the vibrational absorption bands due to water and O-H bound in the near infrared region of the spectrum overlap with atmospheric water and $CO_2$, compromising the mineralogical deconvolution. The standard processing approach to remove the atmospheric contribution is to divide the surface reflectance data by a scaled atmospheric spectrum measured across Olympus Mons, and to suppress the residual errors by dividing the target spectrum by a low spectral contrast reference spectrum of the same session apparently without any relevant features. This method assumes that any instrumental contaminations, as well atmospheric residuals, affect in the same way the two considered spectra. The SAS method based on the principal component analysis and target transformation removes the noise and atmospheric gaseous components from the reflectance spectra, thus allowing to deeply investigate hydrated minerals on the Martian surface. Moreover, the contribution of dust in the atmosphere is also removed by modeling its effect on each spectrum. We first apply the SAS method on a simulated spectral population in order to evaluate its accuracy and then on two OMEGA orbits where hydrated minerals have been already found. The surface reflectance obtained with the SAS method is almost free from instrumental noise and residuals due to atmospheric components (gases and aerosols) are removed.

The surface reflectances obtained for two sessions of observations over Nili Fossae and Mawrth Vallis regions have been investigated by means of MGM, comparing the results obtained from spectra of the same pixel after MO and SAS treatment. In particular, surface spectra showing the hydrated phase have been selected because the diagnostic vibrational absorptions of these minerals are superimposed to the atmospheric absorptions. The information on mineralogy is obtained considering laboratory data, which allows to define the different electronic and vibrational processes to be compared with the measured spectra at Mars. Absorptions between 0.8-1.2 μm can be assigned to electronic $Fe^{2+}$ transitions, both in mafic silicates and in iron-bearing hydrated phases, while absorptions at higher wavelengths reveal the presence in the spectra of overtones of the OH group, in particular Al-OH and Mg-OH overtones. Moreover spectra treated with SAS show a better definition of overtone processes after MGM application, showing a clear reduction of the level of the atmospheric residuals in the 1.8-2.1 μm spectral range. This residual reduction permits

to better define the vibration processes indicative of the hydrate minerals present in remote sensing data and improve the comparison with laboratory data.

As a further application of our work, we will apply the SAS (including the dust correction) method and MGM to the different surface conditions present on Mars.

**Acknowledgements**

We thank the Italian Institute of Astrophysics INAF for the financial support within the project PRIN-INAF 2011. We are thankful to OMEGA team and ESA staff for scientific, operational and technical supports.

## References

Arvidson, R. E.; Poulet F.; Bibring, J.-P.; Wolff, M.; Gendrin, A.; Morris, R.V.; Freeman, J.J.; Langevin, Y.; Mangold, N.; and Bellucci G., 2005. Spectral reflectance and morphologic correlations in eastern Terra Meridiani, Mars. Science, Volume 307, Issue 5715, pp. 1591-1594, doi: 10.1126/science.1109509

Bakker, W. H.; van Ruitenbeek, F. J. A.; van der Werff, H. M. A.; Zegers, T. E.; Oosthoek, J. H. P.; Marsh, S. H.; van der Meer, F. D., 2014. Processing OMEGA/Mars Express hyperspectral imagery from radiance-at-sensor to surface reflectance. Planetary and Space Science, Volume 90, p. 1-9, doi: 10.1016/j.pss.2013.11.007

Bandfield, J. L.; Christensen, P. R.; Smith, M. D., 2000. Spectral data set factor analysis and end-member recovery: Application to analysis of Martian atmospheric particulates. Journal of Geophysical Research, Volume 105, Issue E4, p. 9573-9588, doi: 10.1029/1999JE001094

Bandfield, J.L., Edgett, Kenneth S.; Christensen, Philip R., 2002. Spectroscopic study of the Moses Lake dune field, Washington: Determination of compositional distributions and source lithologies. Journal of Geophysical Research (Planets), Volume 107, Issue E11, pp. 2-1, CiteID 5092, doi: 10.1029/2000JE001469

Bibring, J.P.; Soufflot, A.; Berthé, M.; Langevin, Y.; Gondet, B.; Drossart, P.; Bouyé, M.; Combes, M.; Puget, P.; Semery, A.;and 33 coauthors, 2004. OMEGA: Observatoire pour la Minéralogie, l'Eau, les Glaces et l'Activité. Mars Express: the scientific payload. Ed. by Andrew Wilson, scientific coordination: Agustin Chicarro. ESA SP-1240, Noordwijk, Netherlands: ESA Publications Division, ISBN 92-9092-556-6, 2004, p. 37 - 49

Bibring, J.-P.; Langevin, Y.; Gendrin, A.; Gondet, B.; Poulet, F.; Berthé, M.; Soufflot, A.; Arvidson, R.; Mangold, N.; Mustard, J.; and 32 coauthors, 2005. Mars Surface Diversity as

Revealed by the OMEGA/Mars Express Observations. Science, Volume 307, Issue 5715, pp. 1576-1581, doi: 10.1126/science.1108806

Bishop J.L.; Murad E.; Dyar M.D., 2002a. The influence of octahedral and tetrahedral cation substitution on the structure of smectites and serpentines as observed through infrared spectroscopy. Clay Minerals, 37, 617_628.

Bishop, J. L.; Noe Dobrea, E.Z.; McKeown, N.K.; Parente, M.; Ehlmann, B.L.; Michalski, J.R.; Milliken, R.E.; Poulet, F.; Swayze, G.A.; Mustard, J.F.; and 2 coauthors, 2008. Phyllosilicate Diversity and Past Aqueous Activity Revealed at Mawrth Vallis, Mars. Science, Volume 321, Issue 5890, pp. 830-833, doi: 10.1126/science.1159699

Bishop, J.L.; Lane, M.D.; Dyar, M.D.; Brown, A.J., 2008. Reflectance and emission spectroscopy study of four groups of phyllosilicates: smectites, kaolinite-serpentines, chlorites and micas. Clay minerals, 43, 35-54.

Carrozzo, F. G.; Altieri, F.; Bellucci, G.; Poulet, F.; D'Aversa, E.; Bibring, J.-P., 2012. Iron mineralogy of the surface of Mars from the 1 μm band spectral properties. Journal of Geophysical Research, Volume 117, CiteID E00J17, doi: 10.1029/2012JE004091

Clancy, R. T.; Sandor, B. J.; Wolff, M. J.; Christensen, P. R.; Smith, M. D.; Pearl, J. C.; Conrath, B. J.; Wilson, R. J., 2000. An intercomparison of ground-based millimeter, MGS TES, and Viking atmospheric temperature measurements: Seasonal and interannual variability of temperatures and dust loading in the global Mars atmosphere. Journal of Geophysical Research, Volume 105, Issue E4, p. 9553-9572, doi: 10.1029/1999JE001089

Clark, R.N.; Swayze, G.A.; Gallagher, A.J.; King, T.V.V.; Calvin, W.M., 1993. The U. S. Geological Survey, Digital Spectral Library: Version 1: 0.2 to 3.0 microns, U.S. Geological Survey Open File Report 93-592, 1340 pages.

Clénet, H.; Pinet, P.; Daydou, Y.; Heuripeau, F.; Rosemberg, C.; Baratoux, D.; Chevrel, S., 2011. A new systematic approach using the Modified Gaussian Model: insight for the characterization of chemical composition of olivines, pyroxenes and olivine-pyroxene mixtures. Icarus, 213, 404-422, doi: 10.1016/j.icarus.2011.03.002

Clenet, H.; Pinet, P.; Ceuleneer, G.; Daydou, Y.; Heuripeau, F.; Rosemberg, C.; Bibring, J.-P.; Bellucci, G.; Altieri, F.; Gondet, B. , 2013. A systematic mapping procedure based on the Modified Gaussian Model to characterize magmatic units from olivine/pyroxenes mixtures: Application to the Syrtis Major volcanic shield on Mars. JGR, 118, 1632-1655, doi: 10.1002/jgre.20112

D'Amore, M.; Maturilli, A.; Zinzi, A.; Palomba, E.; Helbert, J., 2013. Martian atmospheric particulate spectral end-members recovery from PFS and IRIS data. Icarus, Volume 226, Issue 2, p. 1294-1303, doi: 10.1016/j.icarus.2013.08.002

Ehlmann, B. L.; Mustard, J. F.; Fassett, C. I.; Schon, S. C.; Head, J. W., III; Des Marais, D. J.; Grant, J. A.; Murchie, S. L., 2008. Clay minerals in delta deposits and organic preservation potential on Mars. Nature Geoscience, Volume 1, Issue 6, pp. 355-358, doi: 10.1038/ngeo207

Ehlmann, B.L.; Mustard, J.F.; Swayze, G.A.; Clark, R.N.; Bishop, J.L.; Poulet, F.; Des Marais, D.J.; Roach, L.H.; Milliken, R.E.; Wray, J.J.; and 2 coauthors, 2009. Identification of hydrated silicate minerals on Mars using MRO-CRISM: Geologic context near Nili Fossae and implications for aqueous alteration. JGR, 114, E00D08, doi: 10.1029/2009JE003339

Forget, F.; Hourdin, F.; Fournier, R.; Hourdin, C.; Talagrand, O.; Collins, M.; Lewis, S.R.; Read, P.L.; Huot, J.-P., 1999. Improved general circulation models of the Martian atmosphere from the surface to above 80 km. Journal of Geophysical Research, Volume 104, Issue E10, p. 24155-24176, doi: 10.1029/1999JE001025

Forget, F.; Spiga, A.; Dolla, B.; Vinatier, S.; Melchiorri, R.; Drossart, P.; Gendrin, A.; Bibring, J.-P.; Langevin, Y.; Gondet, B., 2007. Remote sensing of surface pressure on Mars with the Mars Express/OMEGA spectrometer: 1. Retrieval method. Journal of Geophysical Research, Volume 112, Issue E8, CiteID E08S15, doi: 10.1029/2006JE002871

Gendrin, A.; Mangold, N.; Bibring, J.-P.; Langevin, Y.; Gondet, B.; Poulet, F.; Bonello, G.; Quantin, C.; Mustard, J.; Arvidson, R.; Le Mouélic, S., 2005. Sulfates in Martian Layered Terrains: The OMEGA/Mars Express View. Science, Volume 307, Issue 5715, pp. 1587-1591, doi: 10.1126/science.1109087

Glotch T.D. and Bandfield, J.L., 2006. Determination and interpretation of surface and atmospheric Miniature Thermal Emission Spectrometer spectral end-members at the Meridiani Planum landing site. Journal of Geophysical Research, Volume 111, Issue E12, CiteID E12S06, doi: 10.1029/2005JE002671

Glotch T.D. and Rogers A.D., 2013. Evidence for magma-carbonate interaction beneath Syrtis Major, Mars. Journal of Geophysical Research: Planets, Volume 118, Issue 1, pp. 126-137, doi: 10.1029/2012JE004230

Hamilton, V.E. and Ruff, S.W., 2012. Distribution and characteristics of Adirondack-class basalt as observed by Mini-TES in Gusev crater, Mars and its possible volcanic source. Icarus, Volume 218, Issue 2, p. 917-949, doi: 10.1016/j.icarus.2012.01.011

Hopke, P. K., 1989. Target transformation factor analysis. Chemometrics Intell. Lab. Syst., 6, 7-19.

Ignatiev, N. I.; Grassi, D.; Zasova, L. V., 2005. Planetary Fourier spectrometer data analysis: Fast radiative transfer models. Planetary and Space Science, Volume 53, Issue 10, p. 1035-1042, doi: 10.1016/j.pss.2004.12.009

Klassen, D.R., 2009. Principal components analysis of Mars in the near-infrared. Icarus, Volume 204, Issue 1, p. 32-47, doi: 10.1016/j.icarus.2009.03.041

Klima, R.L.; Pieters, C.M.; Dyar, M.D., 2007. Spectroscopy of synthetic Mg-Fe pyroxenes I: Spin

742 allowed and spin-forbidden crystal field bands in the visible and near-infrared. Meteoritics &
743 Planetary Science 42, 235–253, doi: 10.1111/j.1945-5100.2007.tb00230.x
744
745 Klima, R.L.; Dyar, M.D.; Pieters, C.M., 2011. Near-infrared spectra of clinopyroxenes: Effects of
746 calcium content and crystal structure. Meteoritics & Planetary Science 46, 379–395, doi:
747 10.1111/j.1945-5100.2010.01158.x
748
749 Langevin, Y.; Poulet, F.; Bibring, J.-P.; Gondet, B., 2005. Sulfates in the North Polar Region of
750 Mars Detected by OMEGA/Mars Express. Science, Volume 307, Issue 5715, pp. 1584-1586, doi:
751 10.1126/science.1109091
752
753 Lewis, S.R.; Collins, M.; Read, P.L.; Forget, F.; Hourdin, F.; Fournier, R.; Hourdin, C.;
754 Talagrand, O.; Huot, J.-P., 1999. A climate database for Mars. Journal of Geophysical Research,
755 Volume 104, Issue E10, p. 24177-24194, doi: 10.1029/1999JE001024
756
757 Loizeau, D.; Mangold, N.; Poulet, F.; Bibring, J.-P.; Gendrin, A.; Ansan, V.; Gomez, C.;
758 Gondet, B.; Langevin, Y.; Masson, P.; Neukum, G., 2007. Phyllosilicates in the Mawrth Vallis
759 region of Mars. Journal of Geophysical Research, Volume 112, Issue E8, doi:
760 10.1029/2006JE002877
761
762 Mangold, N.; Poulet, F.; Mustard, J. F.; Bibring, J.-P.; Gondet, B.; Langevin, Y.; Ansan, V.;
763 Masson, Ph.; Fassett, C.; Head, J. W.; and 2 coauthors, 2007. Mineralogy of the Nili Fossae region
764 with OMEGA/Mars Express data: 2. Aqueous alteration of the crust. Journal of Geophysical
765 Research, Volume 112, Issue E8, doi: 10.1029/2006JE002835
766
767 McGuire, P. C.; Bishop, J. L.; Brown, A. J.; Fraeman, A. A.; Marzo, G. A.; Frank Morgan, M.;
768 Murchie, S. L.; Mustard, J. F.; and 7 coauthors, 2009. An improvement to the volcano-scan
769 algorithm for atmospheric correction of CRISM and OMEGA spectral data. Planetary and Space
770 Science, Volume 57, Issue 7, p. 809-815, doi: 10.1016/j.pss.2009.03.007
771
772 Michalski, J.; Poulet, F.; Bibring, J.-P.; Mangold, N., 2010. Analysis of phyllosilicate deposits in
773 the Nili Fossae region of Mars: Comparison of TES and OMEGA data. Icarus, Volume 206, Issue
774 1, p. 269-289, doi: 10.1016/j.icarus.2009.09.006
775
776 Milliken, R. E.; Swayze, G. A.; Arvidson, R. E.; Bishop, J. L.; Clark, R. N.; Ehlmann, B. L.;
777 Green, R. O.; Grotzinger, J. P.; Morris, R. V.; Murchie, S. L.; and 2 coauthors, 2008. Opaline silica
778 in young deposits on Mars. Geology, vol. 36, Issue 11, p.847-850.
779
780 Murchie, S.; Arvidson, R.; Bedini, P.; Beisser, K.; Bibring, J.-P.; Bishop, J.; Boldt, J.; Cavender, P.;
781 Choo, T.; Clancy, R. T.; and 40 coauthors, 2007a. Compact Reconnaissance Imaging Spectrometer
782 for Mars (CRISM) on Mars Reconnaissance Orbiter (MRO), Journal of Geophysical Research,
783 Volume 112, Issue E5, E05S03, doi: 10.1029/2006JE002682.
784
785 Mustard, J. F., et al., 2005. Olivine and Pyroxene Diversity in the Crust of Mars. Science, 307,
786 1594-1597.

Mustard, J. F.; Poulet, F.; Head, J. W.; Mangold, N.; Bibring, J.-P.; Pelkey, S. M.; Fassett, C. I.; Langevin, Y.; Neukum, G., 2007. Mineralogy of the Nili Fossae region with OMEGA/Mars Express data: 1. Ancient impact melt in the Isidis Basin and implications for the transition from the Noachian to Hesperian. Journal of Geophysical Research, Volume 112, Issue E8, doi: 10.1029/2006JE002834

Noe Dobrea, E. Z.; Bishop, J. L.; McKeown, N. K.; Fu, R.; Rossi, C. M.; Michalski, J. R.; Heinlein, C.; Hanus, V.; Poulet, F.; Mustard, R. J. F.; and 6 coauthors, 2010. Mineralogy and stratigraphy of phyllosilicate-bearing and dark mantling units in the greater Mawrth Vallis/west Arabia Terra area: Constraints on geological origin. Journal of Geophysical Research, Volume 115, Issue E11, doi: 10.1029/2009JE003351

Ody, A.; Poulet, F.; Langevin, Y.; Bibring, J.-P.; Bellucci, G.; Altieri, F.; Gondet, B.; Vincendon, M.; Carter, J.; Manaud, N., 2012. Global maps of anhydrous minerals at the surface of Mars from OMEGA/MEx. Journal of Geophysical Research, Volume 117, CiteID E00J14, doi: 10.1029/2012JE004117

Pelkey, S. M.; Mustard, J. F.; Murchie, S.; Clancy, R. T.; Wolff, M.; Smith, M.; Milliken, R.; Bibring, J.-P.; Gendrin, A.; Poulet, F.; and 2 coauthors, 2007. CRISM multispectral summary products: Parameterizing mineral diversity on Mars from reflectance. Journal of Geophysical Research, Volume 112, Issue E8, CiteID E08S14, doi: 10.1029/2006JE002831

Poulet, F.; Bibring, J.-P.; Mustard, J. F.; Gendrin, A.; Mangold, N.; Langevin, Y.; Arvidson, R. E.; Gondet, B.; Gomez, C., 2005. Phyllosilicates on Mars and implications for early martian climate. Nature, Volume 438, Issue 7068, pp. 623-627, doi: 10.1038/nature04274

Poulet, F.; Mangold, N.; Loizeau, D.; Bibring, J.-P.; Langevin, Y.; Michalski, J.; Gondet, B., 2008. Abundance of minerals in the phyllosilicate-rich units on Mars. Astronomy and Astrophysics, Volume 487, Issue 2, doi: 10.1051/0004-6361:200810150

Serventi, G.; Carli, C.; Sgavetti, M. Spectral variability of plagioclase-mafic mixtures (3): quantitative analysis applying the MGM algorithm. Submitted on Icarus

Sgavetti, M.; Serventi, G.; Tampella, G.; Pedrazzi, G.; Carli, C.; Pompilio, L.; Franchi, F.; Tellini, C., 2015. Spectral reflectance characteristics of the Hamar Laghdad hydrothermal sequence, Morocco: Implications for the methane origin on Mars. Icarus, Volume 245, p. 184-197, doi: 10.1016/j.icarus.2014.09.027

Smith, M.D., Bandfield, J.L., Christensen, P.R., 2000. J. Geophys. Res. 105, 9589-9607. doi:10.1029/1999JE001105

Smith, M.D., 2004. Interannual variability in TES atmospheric observations of Mars during 1999-2003. Icarus, Volume 167, Issue 1, p. 148-165, doi: 10.1016/j.icarus.2003.09.010

Sunshine, J.M.; Pieters, C. M.; Pratt, S.F., 1990. Deconvolution of mineral absorption bands: an improved approach. J. Geophys. Res., Vol. 95, 6955-6966. Doi: 10.1029/JB095iB05p06955

Sunshine, J.M.; Pieters, C. M., 1993. Estimating modal abundances from the spectra of natural and laboratory pyroxene mixtures using the Modified Gaussian Model. J. Geophys. Res., Vol. 98, 9075-9087, doi: 10.1029/93JE00677

Sunshine, J.M., Pieters, C. M., 1998. Determining the composition of olivine from reflectance spectroscopy. J. Geophys. Res., Vol. 103, 13675-13688, doi: 10.1029/98JE01217

Thomas, N. H.; Bandfield, J. L.,2013. Identification of Spectral Endmembers in CRISM Data Using Factor Analysis and Target Transformation. 44th Lunar and Planetary Science Conference, held March 18-22, 2013 in The Woodlands, Texas. LPI Contribution No. 1719, p.1325

Thomas, N.H., Bandfield, J.L., Amador, E.S., 2014. Identification and Characterization of Martian Serpentine Using Target Transformation and CRISM Data. 45th Lunar and Planetary Science Conference, held 17-21 March, 2014 at the Woodlands, Texas. LPI Contribution No. 1777, p.1909.

Vincendon, M.; Langevin, Y.; Poulet, F.; Bibring, J.-P.; Gondet, B., 2007. Recovery of surface reflectance spectra and evaluation of the optical depth of aerosols in the near-IR using a Monte Carlo approach: Application to the OMEGA observations of high-latitude regions of Mars. Journal of Geophysical Research, Volume 112, Issue E8, doi: 10.1029/2006JE002845

Wolff, M. J.; Smith, M. D.; Clancy, R. T.; Arvidson, R.; Kahre, M.; Seelos, F.; Murchie, S.; Savijärvi, H., 2009. Wavelength dependence of dust aerosol single scattering albedo as observed by the Compact Reconnaissance Imaging Spectrometer. Journal of Geophysical Research, Volume 114, Issue E9, CiteID E00D04, doi: 10.1029/2009JE003350

***Highlights (for review)**

- We retrieve the surface component from near-IR reflectance spectra.
- We apply the principal component analysis and target transformation to OMEGA spectra.
- Atmospheric dust is removed by means of a radiative transfer model.
- A test spectral population is used to validate the method used in this work.
- MGM analysis shows an improved match of our result with laboratory analogues.